Atmos. Chem. Phys. Discuss., 9, 16051–16083, 2009
www.atmos-chem-phys-discuss.net/9/16051/2009/

Atmospheric Chemistry and Physics Discussions

This discussion paper is/has been under review for the journal *Atmospheric Chemistry and Physics (ACP)*. Please refer to the corresponding final paper in *ACP* if available.

The influence of the vertical distribution of emissions on tropospheric chemistry

A. Pozzer[1,2], **P. Jöckel**[2], **and J. Van Aardenne**[3]

[1]The Cyprus Institute, Energy, Environment and Water Research Centre, Nicosia, Cyprus
[2]Max-Planck Institute of Chemistry, Air Chemistry Department, Mainz, Germany
[3]European Commission, DG Joint Research Centre, Ispra, Italy

Received: 22 June 2009 – Accepted: 7 July 2009 – Published: 28 July 2009

Correspondence to: A. Pozzer (pozzer@cyi.ac.cy)

Published by Copernicus Publications on behalf of the European Geosciences Union.

Abstract

The atmospheric chemistry general circulation model EMAC (ECHAM5/MESSy atmospheric chemistry) is used to investigate the effect of height dependent emissions on tropospheric chemistry. In a sensitivity simulation, anthropogenic and biomass burning emissions are released in the lowest model layer. The resulting tracer distributions are compared to those of a former simulation applying height dependent emissions. Although the differences between the two simulations in the free troposphere are small (less than 5%), large differences are present in polluted regions at the surface, in particular for NO_x (more than 100%) and non-methane hydrocarbons (up to 30%), whereas for OH the differences at the same locations are somewhat lower (15%). Global ozone formation is virtually unaffected by the choice of the vertical distribution of emissions. Nevertheless, local ozone changes can be up to 30%. Model results of both simulations are further compared to observations from field campaigns and to data from measurement stations. The two simulations show no significant differences when compared to aircraft observations. In contrast, for measurements from surface stations, the simulation with emissions in the lowest model layer gives a 20% lower correlation to the observations compared to the simulation with height dependent emissions.

1 Introduction

Emission data are essential for a realistic simulation of the chemistry in chemistry climate models. Accurate emission data require an appropriate spatial and temporal resolution. Although the spatial resolution is generally confined in a two-dimensional representation, the vertical distribution of the emissions is also an information which needs to be addressed. This topic is well known and a plethora of case studies show the importance of a correct vertical distribution of biomass burning plume emissions for a realistic representation of tracers and aerosols (Fromm et al., 2000; Jost et al., 2004; Fromm et al., 2005; Luderer et al., 2006). For global chemistry models, a simple and

ACPD

9, 16051–16083, 2009

computationally affordable method is to arbitrarily distribute the emissions throughout the tropospheric column (e.g. Cook et al., 2007; Pfister et al., 2005; Matichuk et al., 2007; Generoso et al., 2007) Recently, more sophisticated approaches have been used, with an online calculation of injection heights based on thermodynamics calculations (Freitas et al., 2006; Hodzic et al., 2007).

Unlike the role of biomass burning plume emissions, the importance of the vertical distribution of anthropogenic emissions for a correct tracer representation in global models is still unclear. For these kind of emissions, only a few studies on the measurements of emission heights exist (see Pregger and Friedrich, 2009, and references therein). Hence, three-dimensional models have to rely on simple assumptions on the height dependency of the anthropogenic emissions. Furthermore, also in the emission models, information on the vertical distribution has only very recently and/or only partly been implemented (Friedrich et al., 2000). Pregger and Friedrich (2009) showed that this is a major issue in regional/urban models. Moreover, they showed that the distribution of the emissions into different model layers is particularly important for large sources, which also play a major role in global models.

In this study two different simulations, one with emissions in the lowest model layer and one with a height dependent emission distribution are compared. After a description of the model setup, resulting differences in the distribution of the reactive nitrogen family, (NO_x=NO+NO_2, NO_y=NO+NO_2+HNO_3+PAN, peroxyacetylnitrate), the hydroxyl radical (OH), ozone (O_3) and non-methane hydrocarbons (NMHC) are analysed. Finally, results from the two simulations are compared to aircraft and station measurements. It is shown that the choice of the vertical distribution of the emissions into different model layers is essential for a correct representation of the chemistry in the planetary boundary layer in polluted regions.

ACPD
9, 16051–16083, 2009

2 Model description and setup

The ECHAM5/MESSy atmospheric chemistry (EMAC) model is a combination of the general circulation model ECHAM5 (Roeckner et al., 2006, version 5.3.01) and the Modular Earth Submodel System (Jöckel et al., 2005, MESSy; version 1.1). The description and evaluation of the model system has been published (Jöckel et al., 2006). More details about the model system can also be found at http://www.messy-interface.org, where a comprehensive description of the model is provided.

The results evaluated here are based on data from the reference simulation S1, as described by Jöckel et al. (2006). The simulation period covers almost 8 years from January 1998 to October 2005. Dry and wet deposition processes have been extensively described by Kerkweg et al. (2006a) and Tost et al. (2006), respectively. The emission procedure has been explained by Kerkweg et al. (2006b). The chemistry is calculated with the MECCA submodel (Sander et al., 2005). The applied spectral resolution of the ECHAM5 base model is T42, corresponding to a horizontal resolution of the quadratic Gaussian grid of approximately $2.8^{\circ} \times 2.8^{\circ}$. The applied vertical resolution consists of 90 levels (up to about 80 km) of which about 25 are located in the troposphere. The model setup includes feedbacks between chemistry and dynamics via the radiation calculations. The model dynamics has been weakly nudged (Jeuken et al., 1996; Jöckel et al., 2006; Lelieveld et al., 2007) towards the analysis data of the ECMWF operational model (up to 100 hPa) in order to represent the realistic meteorology in the troposphere. This allows a direct comparison with observations. For more details on the model setup we refer to Jöckel et al. (2006). Here, we repeat briefly the setup of the emissions.

We used the anthropogenic emissions from the EDGAR database (van Aardenne et al., 2005, version 3.2 "fast-track") for the year 2000 as described by Pozzer et al. (2007). The emissions were, depending on the emission class and species, distributed to 6 different heights (45, 140, 240, 400, 600 and 800 m above ground). The chosen vertical distribution of the emissions is partly based on experiences from the EMEP

ACPD
9, 16051–16083, 2009

model (Dimitroulopoulou and ApSimon, 1999; Simpson et al., 2003), applied after the analysis of some stack data from Eastern Europe. These vertically distributed emissions are based on the "effective" emissions, i.e. the effective elevation where the emissions take part. The detailed vertical distribution by emission class is listed in the electronic supplement (http://www.atmos-chem-phys-discuss.net/9/16051/2009/acpd-9-16051-2009-supplement.pdf). Biogenic emissions, which are not on-line calculated (except for NO_x), are prescribed at the surface (lowest model layer) for all species and do not have any vertical distribution. NO_x produced by lighting is distributed on different vertical levels, based on the parametrization of Price and Rind (1992).

The biomass burning contribution was added using the Global Fire Emissions Database (GFED version 1, Van der Werf et al., 2004) for the year 2000. No interannual variability is present for biomass burning. In addition, biomass burning emissions are located exclusively at 140 m elevation. Colarco and Andreae (2004) suggested a much higher injection for boreal fires, while Ferguson et al. (2003) estimated a lower value for smouldering fires. In addition, Labonne et al. (2007) showed that for the majority of the global biomass burning activity, the injection occurs in the mixing layer, and direct injection into the free troposphere is a rare phenomenon. Langmann et al. (2009, and references therein) concluded that most of the fires deposit their emissions in the PBL, and only in a few cases (i.e. under specific fire and meteorological conditions), the emissions are located in the upper troposphere or even in the lower stratosphere. Focusing mainly on the role of anthropogenic emissions, we applied a common constant emission height of 140 m altitude for biomass burning emissions. This altitude, in fact, implies that more than 60% of the biomass burning emissions are within the PBL (see Fig. 1), depending on the meteorological conditions.

In Table 1 the total emissions are summarised, including their distribution on the six vertical levels. Moreover, for the reference year 2000 the total amounts emitted above the Planetary Boundary Layer (PBL) are listed. As Table 1 shows, around 20% of the total carbon monoxide is directly emitted into the free troposphere. In Fig. 1, the geographical distribution of the CO emissions outside the PBL is depicted. Strong

ACPD
9, 16051–16083, 2009

sources are present in central Africa, India and partially China and the Amazonian basin, whereas in North America, Europe and Australia emissions outside the PBL are smaller.

The effect of vertically distributed emissions on the global distribution of trace species is investigated with an additional simulation, further denoted as F1. For simulation F1 we applied the same executable used in simulation S1, and the same model setup. As only difference, the namelist of the offline-emissions submodel (submodel OFFLEM) was altered in order to emit the species entirely in the lowest model layer, i.e. without any height dependency. This modification applies to NO, CO, C_2H_4, C_2H_6, C_3H_6, C_3H_8, C_4H_10, CH_3CHO, CH_3COCH_3, CH_3COOH, CH_3OH, HCHO, HCOOH and MEK. Because simulation F1 is nudged toward ECMWF analysis data, the meteorology is comparable to the one in simulation S1. This implies that the on-line emissions (due to biogenic processes) and the NO + NO_2 produced by lightning are similar in both simulations.

For the analysis we focus on the year 2000, which is expected to be represented by the model with the highest consistency, mainly because the chosen emission database was compiled for this year. In addition, simulation S1 has already been extensively evaluated using the model output of the year 2000 (Pozzer et al., 2007).

3 The global distribution of selected compounds

3.1 Reactive Nitrogen: NO_x, HNO_3 and PAN

In the troposphere the reactive nitrogen compounds play a key role in the ozone formation and in the recycling of the hydroxyl radical. While the NO_x family ($NO+NO_2$) is important for these processes, HNO_3 and PAN (peroxyacetylnitrate) are reaction products and reservoir species. HNO_3 represents one of the main sinks of reactive nitrogen through its washout, and PAN represents an important NO_x source in remote regions due to its temperature dependent stability. Changing the vertical distribution of the

ACPD
9, 16051–16083, 2009

emissions by removing the height dependency, drastically increases the NO_x mixing ratios at the surface (lowest model layer), with about a factor of 2 to 3 higher NO_x mixing ratios in simulation F1 compared to simulation S1. This increase is compensated by a strong decrease in the PBL above the surface model layer, where simulation F1 results in 10–20% lower mixing ratios than simulation S1. As shown in Table 2, the emissions into the lowest model layer (simulation F1) result in a more efficient dry deposition of the $NO+NO_2$. For the very reactive NO_x, the dry deposition in simulation F1 (5.5 Tg(N)/year) is almost double (67% larger) the dry deposition in simulation S1 (3.3 Tg(N)/year). Although this does not significantly change the global view of the NO_y distribution, other compounds (e.g. O_3) are influenced by the strong changes in the dry deposition of NO_x.

The global burden of PAN, which is thermally unstable, is reduced (~ 5%) due to a reduced formation near the surface, where the temperature is higher than higher up in the PBL or free troposphere. This decreased burden reduces the transport into remote areas and there the production of NO_x by thermal decomposition of PAN.

The two model simulations show different characteristics for different regions (see Fig. 2). Compared to simulation S1,

- at the surface, simulation F1 shows an increase of NO_x (more than 100%) in polluted regions and a decrease of NO_y in remote regions (3–10%),
- in the PBL, simulation F1 shows a decrease of NO_x due to the absence of emissions in the PBL above the surface in both, polluted and remote regions,
- in the free troposphere, simulation F1 shows a decrease of NO_x and NO_y (1–5%).

An overall reduction of the reactive nitrogen species at locations away from the sources is apparent in simulation F1 compared to simulation S1.

ACPD
9, 16051–16083, 2009

3.2 Oxidation capacity

The HO_x family ($OH+HO_2$) and the NO_x family are strongly coupled, mainly through the reaction $NO+HO_2 \rightarrow NO_2+OH$, leading to the recycling of OH and (with the photolysis of NO_2) to the formation of ozone. Since simulation F1 predicts higher NO_x mixing ratios at the surface in polluted regions, the OH mixing ratios are up to 20–30% higher than in simulation S1. Consistently, the HO_2 mixing ratios are lower by about 30–40%.

Due to the lower mixing ratios of NO_x in simulation F1 in the remote regions (surface, PBL and free troposphere), the recycling of OH is less efficient. This induces a decreased mixing ratio of OH by 2 to 6%. As shown in Fig. 3, the zonal average decrease is overall about 5% and about 10% in the PBL over the northern subtropics, where the emissions are large. In conclusion, although with height-independent emissions OH increases locally in polluted regions at the surface, the oxidation capacity of the atmosphere is globally reduced.

3.3 Carbon monoxide, CO

Carbon monoxide provides the most important sink for OH (Lelieveld et al., 2002; Logan et al., 1981; Thompson, 1992). A correct simulation of this tracer is very important for the assessment of atmospheric oxidants.

The CO emissions change from 492 Tg/year at the lowest model level in simulation S1 to 1096 Tg/year in simulation F1 (see Table 1). The differences between simulation S1 and simulation F1 apparent for CO are also present for the alkanes (C_2H_6 and C_3H_8, not shown) and the alkenes (C_2H_4 and C_3H_6, not shown).

In simulation F1, all emissions are concentrated at the surface. The mixing ratios at the surface are therefore larger in simulation F1 as in simulation S1, despite the enhanced OH induced by the increased recycling of OH due to the higher mixing ratio of NO_x. As shown in Fig. 4, the differences in polluted regions (especially where strong biomass burning emissions occur) can be larger than 30%. Nevertheless, because of the CO transported outside the polluted regions, simulation F1 results in lower OH

ACPD
9, 16051–16083, 2009

mixing ratios compared to simulation S1 (see Sect. 3.2). This implies also a reduce oxidation of CO and NMHCs. As a consequence, in remote regions the mixing ratios of CO in simulation F1 are higher than in simulation S1. It must be stressed that the differences for remote conditions are comparably small, only about 1–3% on annual average (see Fig. 4). In summary, at the surface simulation F1 shows a global increase of CO, ranging from about 30% in polluted regions to about 3% in remote regions.

In the PBL and the free troposphere the situation is similar. In polluted regions simulation S1 shows higher mixing ratios for CO, as it does for NO_x. This is restricted, however, to locations where strong emissions within the PBL are present (Central Africa, East India, Amazonia). In fact, the comparable long lifetime of CO allows a very effective mixing. This, in combination with the reduced OH abundance in simulation F1 causes higher mixing ratios of CO at almost all locations. Hence, with the exception of a few locations, CO is everywhere slightly (1–3%) higher in the PBL and the free troposphere in simulation F1 compared to simulation S1.

3.4 Ozone O_3

Ozone chemistry in the troposphere is highly dependent on precursor species like NO_x(=NO+NO_2), CO and NMHCs (Atkinson, 2000; Logan, 1985; Houweling et al., 1998; Seinfeld and Pandis, 1997). Although simulation S1 and simulation F1 show very low differences in the free troposphere and in remote regions, large differences arise over polluted regions at the surface and in the PBL. In Table 3 the ozone production and loss terms are listed for simulation S1 and simulation F1. The results for the two simulations are comparable in terms of production and transport. This implies that the net exchange between troposphere and stratosphere (and likewise between the free troposphere and the PBL) is hardly influenced by the choice of the vertical distribution of emissions. The stratosphere-troposphere exchange (STE) of ozone changes only by 3% between the two simulations (10 Tg/year). This is less than the inter-annual variability of the STE of ozone simulated by the model, which is about 25 Tg/year (Jöckel et al., 2006). Also in the PBL the production and loss terms are similar in simulation F1

ACPD
9, 16051–16083, 2009

and simulation S1. This implies that the total amount of ozone produced is the same in both simulations, although the production is localised differently.

On the local scale, however, differences between the two simulations of up to 30% arise in polluted regions. In simulation F1, O_3 production is reduced at the surface in polluted regions in comparison to simulation S1.

4 Comparison with observations

To provide an overview of the model performance for simulation S1 and simulation F1, a statistical comparison between observations and model results is presented. Observations are taken from a collection of aircraft measurements (Emmons et al., 2000) and from a large number of multi-year surface measurements collected from the literature. The aircraft data provide information about the vertical distribution of many tracers (although for relatively short periods) and the station data about the seasonality of the same tracers at the surface. An additional global dataset of surface measurements is the NOAA/ESSL flask sampling network (Novelli et al., 1998), which encompasses several years of CO measurements. For a quantitative statistical analysis, correlations between the model results and the aircraft observations are calculated with respect to the altitude, while the correlations between the model results and the surface measurements are calculated with respect to time.

4.1 Comparison with aircraft measurements

Table 4 summarises the comparison of model results from simulation S1 and simulation F1 with measurements on board of aircraft. The majority of the measurements included in this study have been collected in remote regions or downwind of polluted regions, where, as shown in Sects. 3.1–3.4, the differences between simulation S1 and simulation F1 are small or in the range of the measurements variabilities. In fact, no significant differences between the two simulations are found when they are compared

ACPD
9, 16051–16083, 2009

with these aircraft observations. In the measurement regions, the vertical distributions of these tracers show the same patterns and the same magnitude. The correlation between simulation S1 and the observations is overall larger (see C_2H_4 and C_3H_6) or equal to (C_2H_6, C_4H_8, CH_3COCH_3, H_2O_2, HNO_3, O_3 and NO) than the respective correlation calculated between the results of simulation F1 and the observations.

Since the aircraft campaigns took mainly place in remote regions, significant differences between simulation S1 and simulation F1 occur only at a few locations (see Fig. 4). Only few aircraft campaigns present in the dataset include polluted/partially polluted regions. An example is presented in Fig. 5, where vertical profiles at a polluted location (left, TOPSE-May, Churchill) and at a location downwind of a polluted region (right, TRACE-P, China) are shown. The mixing ratios at the surface calculated from simulation F1 are larger than those from simulation S1 (a factor of 3 in TRACE-P, China). In contrast, between 600 m and ~1.5 km altitude, the opposite is visible, the mixing ratios from simulation S1 being larger than those from simulation F1 (see Sect. 3.1). Moreover, at the surface (see Fig. 5, TRACE-P, China), simulation S1 is closer to the observed value, which is the average of 389 measurements taken during the campaign period in the region at that level. In the free troposphere, however, no substantial differences are noticeable between the two simulations.

In Fig. 6, results for CO from both simulations are compared with measurements from the TRACE-A field campaign (Talbot et al., 1996). The same differences between the two simulations discussed above for NO are also present for CO. In Fig. 6 a comparably large difference between simulation S1 and simulation F1 in the PBL and an insignificant difference in the free troposphere is apparent. This confirms the low (less than 2%) sensitivity of the trace gas distributions to the vertical distribution of emissions in remote regions and the free troposphere shown in Sect. 3. In particular, the measurements at the surface (see TRACE-A, E-Brazil) show that simulation S1 better represents CO in this region than simulation F1. The Trace-A campaign took place during the Southern Hemisphere dry season and some flights were influenced by biomass burning (Talbot et al., 1996). It can be concluded that the vertical distribu-

ACPD
9, 16051–16083, 2009

tion of the emissions (simulation S1) yields more realistic results than the setup with emissions confined to the surface layer (simulation F1). This confirms previous findings (see Turquety et al., 2007, and references therein) that biomass burning emissions should be vertically distributed, although no real indication of an ideal vertical emission distribution can be derived from this comparison.

4.2 Comparison with station observations

A striking different picture arises when simulation S1 and simulation F1 are compared to surface observations. As mentioned in the previous sections (from Sect. 3.1 to Sect. 3.3) simulation F1 shows higher mixing ratios at the surface in polluted regions than simulation S1, in particular for CO, NO_y and HO_x. In contrast to the aircraft measurements, the set of observational sites comprise also stations located in industrialised regions (e.g. Egbert, Canada) or downwind source regions (e.g. Rucava, Latvia), giving the opportunity to evaluate the model at locations where the effect of changing the vertical emissions distributions is large.

As shown in Table 5, results from simulation S1 agree by far better with the observations than the results from simulation F1. The correlations between the tracer mixing ratios of simulation S1 and the observations are 20–30% larger than the respective correlations of simulation F1. Moreover, the bias between simulation S1 and the observations is generally lower (about 30%) than the respective bias of simulation F1, with the exception of acetaldehyde (CH_3CHO) and formaldehyde (HCHO). In the case of acetaldehyde,the model poorly represents this tracer (see Pozzer et al. (2007), confirmed by the very low correlation between model and observations). Hence no real conclusion can be drawn for this specific tracer. In the case of formaldehyde (HCHO), instead, the model is generally representing the observations quite accurately, although with a certain overestimation. The differences between simulation S1 and simulation F1 in bias and correlation for HCHO are due to the different behaviour of the two simulations at Zeppelin (see Fig. 7). In this location, while the correlation of the two simulations with the observations largely differ (the phase of the seasonal cycle of mixing

ACPD
9, 16051–16083, 2009

ratios from simulation F1 and simulation S1 are different), the low values of mixing ratios from simulation F1 balance the general overestimation obtained at other stations, when the bias is calculated. Hence, it can be concluded that the decrease of the bias between observations and simulation F1 compared to simulation S1 is an artefact. In addition, Fig. 7 (Zeppelin station) shows a better agreement of results from simulation S1 than from simulation F1 with the measurements.

Peculiar is acetone (CH_3COCH_3), which is mainly emitted biogenically, with only a few percent contribution of anthropogenic origin (Jacob et al., 2002, and references therein). Hence, the acetone mixing ratio shows differences between simulation S1 and simulation F1 mainly due to indirect effects, such as local changes in the oxidation capacity and/or different degradation of acetone precursors.

Here, we only show ethane (C_2H_6), one of the best simulated tracers in the model (Pozzer et al., 2007). In Fig. 8 observations and model results are compared. The average values are comparable between the two simulations. Differences arise especially during summer, e.g., in Rorvik, Birkenes, or Egbert, where simulation F1 shows larger mixing ratios as simulation S1. Here, results from simulation F1 are in clear contrast to the observations (see Fig. 8).

Also for CO the correlation between station measurements and simulated mixing ratios is higher for simulation S1 than for simulation F1, yet the difference is smaller than for other trace gases. As pointed out by Haas-Laursen and Hartley (1997), the flask samples were supposed to be collected under non-polluted conditions, i.e. for stations close to local sources only certain wind directions have been selected to avoid local contamination. Hence, the effect of the different vertical distributions of emissions is lower for CO at these locations (see also Sect. 3.2). As shown in Fig. 9, results from simulation S1 and simulation F1 hardly differ. It can hence be confirmed that for background conditions the different vertical emissions distributions do not change the simulated surface mixing ratios considerably (about 1%, see Sect. 3.3).

ACPD
9, 16051–16083, 2009

5 Conclusions

The ECHAM5/MESSy atmospheric chemistry (EMAC) general circulation model was used to investigate the effect of height dependent emissions on tropospheric chemistry. Two simulations were performed and the results compared. In one simulation (simulation F1) the anthropogenic and biomass burning emissions were confined to the surface layer, while in the second (simulation S1) the emissions have been distributed vertically to 6 different altitudes. The resulting trace gas distributions of the two simulations do not differ considerably in remote regions and in the free troposphere, with differences of less than 5%. However, large differences occur at the surface in polluted regions, with differences of more than 100%, depending on the species.

A comparison of the model results with data from various aircraft field campaigns and surface stations confirm these results. The field campaigns mainly took place in unpolluted regions, therefore results from both simulations correlate similarly to those observations and no significant difference can be detected. In contrast to this, the correlation of the model results to the surface observations, which include also polluted locations, is significantly (10–30%, depending on the species) reduced, if the emissions are confined to the surface. For alkanes and alkenes, a 20 to 30% percent decrease of the correlation coefficient is calculated, while for CO a decrease of 10% is derived. The lower sensitivity of CO can be traced back to the used database, since the observations in the database have been filtered for non-polluted conditions.

In addition to the improved correlation, also the bias between simulated and observed mixing ratios is reduced, if the emissions are vertically distributed. We conclude that results of an atmospheric chemistry general circulation model in remote regions are hardly affected by the chosen vertical distribution of the emissions, whereas the information about the vertical distribution of emissions is essential to reproduce correctly the chemistry in polluted regions.

To improve the process of emissions in such models, further research is required. A more realistic approach might be to connect the vertical distribution of emissions

ACPD
9, 16051–16083, 2009

consistently to the simulated meteorological situation (e.g. vertical stability). Although some work in this direction has been performed for biomass burning (Freitas et al., 2006, 2007) already, more work on anthropogenic emissions is required. New emission (plume) models have to be applied and many more observations of "real world" emissions are required to further constrain the models.

Acknowledgements. The authors wish to acknowledge the suggestions by the editor B. Duncan for improving the manuscript, P. Zimmermann and T. Butler for preparing the emissions files, H. Riede for comments, and M. Lawrence for valuable suggestions on the manuscript. The authors wish also to acknowledge the use of the Ferret program for analyses and graphics in this paper. Ferret is a product of NOAA's Pacific Marine Environmental Laboratory (information is available at http://www.ferret.noaa.gov).

The service charges for this open access publication
have been covered by the Max Planck Society.

References

Atkinson, R.: Atmospheric chemistry of VOCs and NO_x, Atmos. Environ., 34, 2063–2101, 2000. 16059

Colarco, P. and Andreae, M.: Biomass burning in the tropics: Impact on atmospheric chemistry and biogeochemical cycles, J. Geophys. Res., 109, D06203, doi:10.1029/2003JD004248, 2004. 16055

Cook, P. et al.: Forest fire plumes over the North Atlantic: p-TOMCAT model simulations with aircragt and satellite measurements from the ITOP/ICARTT campaign, J. Geophys. Res., 112, D10S43, doi:10.1029/2006JD007563, 2007. 16053

Dimitroulopoulou, C. and ApSimon, H. M.: The influence of the photolysis rates on modelled ozone concentrations, Atmos. Environ., 33, 147–154, 1999. 16055

Emmons, L. K., Hauglustaine, D.A., Müller, J. F., Carroll, M. A., Brasseur, G. P., Brunner, D., Staehelin, J., Thouret, V., and Marenco, A.: Data composites of airborne observations of tropospheric ozone and its precursors, J. Geophys. Res., 105, 20497–20538, 2000. 16060, 16079

Ferguson, S., Collins, R., Ruthford, J., and Fukuda, M.: Vertical distribution of nighttime smoke following a wildland biomass fire in boreal Alaska, J. Geophys. Res., 108(D23), 4743, doi:10.1029/2002JD003324, 2003. 16055

Freitas, S. R., Longo, K., and Andreae, M.: Impact of including the plume rise of vegetation fires in numerical simulations of associated atmospheric pollutants, Geophys. Res. Lett., 33, L17808, doi:10.1029/2006GL026608, 2006. 16053, 16065

Freitas, S. R., Longo, K., Chatfield, R., Latham, D., Silva Dias, M., Andreae, M., Prins, E., Santos, J., Gielow, R., and Carvalho, J.: Including the sub-grid scale plume rise of vegetation fires in low resolution atmospheric transport models, Atmos. Chem. Phys., 7, 3385–3398, 2007, http://www.atmos-chem-phys.net/7/3385/2007/. 16065

Friedrich, R., Heidegger, A., and Kudermann, F.: Development of an emission calculation module as a part of a model network for regional atmospheric modelling, in: Proceedings of the EUROTRAC Symposium 1998: Garmisch-Partenkirchen, edited by WIT Press, Boston, S., 2000. 16053

Fromm, Bevilaqua, R., Servranckx, R., Rosen, J., Thayer, J., Herman, J., and Larko, D.: Pyro-cumulonimbus injection of smoke to the stratosphere: Observation and impact of a super blowup in northwestern Canada on 3–4 August 1998, J. Geophys. Res., 110, D08205, doi:10.1029/2004JD005350, 2005. 16052

Fromm, M., Alfred, J., Hoppel, K., Hornstein, J., Bevilaqua, R., Shettle, E., Servranckx, R., Z, L., and Stocks, S.: Observation of boreal forest fire smoke in the stratosphere by POAM III, SAGE III and lidar in 1998, Geophys. Res. Lett., 27, 1407–1410, 2000. 16052

Generoso, S., Bey, I., Attie, J. L., and Breon, F. M.: A satellite- and model-based assessment of the 2003 Russian fires: inpact on the Artic region., J. Geophys. Res., 112, D15302, doi:10.1029/2006JD008344, 2007. 16053

Haas-Laursen, D. and Hartley, D.: Consistent sampling methods for comparing models to CO_2 flask data, J. Geophys. Res., 102, 19059–19071, 1997. 16063

Hodzic, A., Madronich, S., Bohn, B., Massie, S., Menut, L., and Wiedinmyer, C.: Wildfire particulate matter in Europe during summer 2003: meso-scale modeling of smoke emissions, transport and radiative effects, Atmos. Chem. Phys., 7, 4043–4064, 2007, http://www.atmos-chem-phys.net/7/4043/2007/. 16053

Houweling, S., Dentener, F., and Lelieveld, J.: The impact of non-methane hydrocarbon compounds on tropospheric photochemistry, J. Geophys. Res., 103, 10673–10696, 1998. 16059

Jacob, D., Field, B., Jin, E., Bey, I., Li, Q., Logan, J., and Yantosca, R.: Atmospheric budget of acetone, J. Geophys. Res., 107, 4100, doi:10.1029/2001JD000694, 2002. 16063

Jeuken, A., Siegmund, P., Heijboer, L., Feichter, J., and Bengtsson, L.: On the potential assimilating meteorological analyses in a global model for the purpose of model validation, J. Geophys. Res., 101, 16939–16950, 1996. 16054

Jöckel, P., Sander, R., Kerkweg, A., Tost, H., and Lelieveld, J.: Technical Note: The Modular Earth Submodel System (MESSy) – a new approach towards Earth System Modeling, Atmos. Chem. Phys., 5, 433–444, 2005, http://www.atmos-chem-phys.net/5/433/2005/. 16054

Jöckel, P., Tost, H., Pozzer, A., Brühl, C., Bucholz, J., L., G., Hoor, P., Kerkweg, A., Lawrence, M., Sander, R., Steil, B., Stiller, G., Tanarhte, M., Taraborrelli, D., van Aardenne, J., and Lelieveld, J.: Evaluation of the atmospheric chemistry GCM ECHAM5/MESSy: Consistent simulation of ozone in the stratosphere and troposphere, Atmos. Chem. Phys., 6, 5067–5104, 2006, http://www.atmos-chem-phys.net/6/5067/2006/. 16054, 16059

Jost, H.-J. et al.: In-situ observations of mid-latitude forest fire plumes deep in the stratosphere, Geophys. Res. Lett., 31, L11101, doi:10.1029/2003GL019253, 2004. 16052

Kerkweg, A., Buchholz, J., Ganzeveld, L., Pozzer, A., Tost, H., and Jöckel, P.: Technical Note: An implementation of the dry removal processes DRY DEPosition and SEDImentation in the Modular Earth Submodel System (MESSy), Atmos. Chem. Phys., 6, 4617–4632, 2006a, http://www.atmos-chem-phys.net/6/4617/2006/. 16054

Kerkweg, A., Sander, R., Tost, H., and Jöckel, P.: Technical Note: Implementation of prescribed (OFFLEM), calculated (ONLEM), and pseudo-emissions (TNUDGE) of chemical species in the Modular Earth Submodel System (MESSy), Atmos. Chem. Phys., 6, 3603–3609, 2006b, http://www.atmos-chem-phys.net/6/3603/2006/. 16054

Labonne, M., Breon, F. M., and Chevallier, F.: Injiection height of biomass burning aerosol as seen from a spaceborne lidar, Geophys. Res. Lett., 34, L11806, doi:10.1029/2007GR029311, 2007. 16055

Langmann, B., Duncan, B., Textor, C., Trentmann, J., and van der Werf, G.: Vegetation fire emissions and their impact on air pollution and climate, Atmos. Environ., 43, 107–116, 2009. 16055

Lelieveld, J., Peters, W., Dentener, F., and Krol, M.: Stability of tropospheric hydroxyl chemistry, J. Geophys. Res., 107, 4715, doi:10.1029/2002JD002272, 2002. 16058

Lelieveld, J., Brühl, C., Steil, B., Crutzen, P., Fischer, H., Giorgietta, M., Hoor, P., Milz, M., Sausen, R., Stiller, G., and Tost, H.: Stratospheric dryness, Atmos. Chem. Phys., 7, 1313–1332, 2007, http://www.atmos-chem-phys.net/7/1313/2007/. 16054

Logan, J. A.: Tropospheric ozone: Seasonal behavior, trends, and anthropogenic influence, J. Geophys. Res., 90, 10463–10482, 1985. 16059

Logan, J. A., Prather, M. J., Wofsy, S. C., and McElroy, M. B.: Tropospheric chemistry: A global perspective, J. Geophys. Res., 86, 7210–7254, 1981. 16058

Luderer, G., Trentmann, J., Winterrath, T., Textor, C., Herzog, M., Graf, H.-F., and Andreae, M.: Modeling of biomass smoke injection into lower stratosphere by a large forest fire: Sensitivity studies, Atmos. Chem. Phys., 6, 5261–5277, 2006, http://www.atmos-chem-phys.net/6/5261/2006/. 16052

Matichuk, R., Cloarco, P., Smith, J., and Toon, O.: Modeling the transport and optical properties of smoke aerosol form African savanna fires during the Southern African Regional Science Initiative campaign (SAFARI 2000), J. Geophys. Res., 112, D08203, doi:10.1029/2006JD007528, 2007. 16053

Novelli, P. C., Masarie, K. A., and Lang, P. M.: Distribution and recent changes of carbon monoxide in the lower troposphere, J. Geophys. Res., 103, 19015–19033, 1998. 16060, 16083

Pfister, G., Hess, P., Emmons, L., Lamarque, J. F., Edwards, D., Petron, G., Gille, J., and Sachse, G.: Quantifying CO emissions from the 2004 Alaskan wildfires using MOPITT CO data, Geophys. Res. Lett., 32, L11809, doi:10.1029/2005GL022995, 2005. 16053

Pozzer, A., Jöckel, P., Tost, H., Sander, R., Ganzeveld, L., Kerkweg, A., and Lelieveld, J.: Simulating organic species with the global atmospheric chemistry general circulation model ECHAM5/MESSy1: a comparison of model results with observations, Atmos. Chem. Phys., 7, 2527–2550, 2007, http://www.atmos-chem-phys.net/7/2527/2007/. 16054, 16056, 16062, 16063

Pregger, T. and Friedrich, R.: Effective pollutant emission heights for atmospheric transport modelling based on real-world information, Environmental Pollution, 157(2), 552–560, doi:10.1016/j.envpol.2008.09.027, 2009. 16053

Price, C. and Rind, D.: A simple lightning parameterization for calculating global lightning distributions, J. Geophys. Res., 97, 9919–9933, 1992. 16055

Roeckner, E., Brokopf, R., Esch, M., Giorgetta, M., Hagemann, S., Kornblueh, L., Manzini, E.,

Schlese, U., and Schulzweida, U.: Sensitivity of simulated climate to horizontal and vertical resolution in the ECHAM5 atmosphere model, J. Clim., 19, 3771–3791, 2006. 16054
Sander, R., Jöckel, P., Kerkweg, A., and Lelieveld, J.: Technical Note: The new comprehensive atmospheric chemistry module MECCA, Atmos. Chem. Phys., 5, 445–450, 2005, http://www.atmos-chem-phys.net/5/445/2005/. 16054
Seinfeld, J. H. and Pandis, S.: Atmospheric Chemistry and Physics: From Air Pollution to Climate Change, Wiley-Interscience, 204–231, 1997. 16059
Simpson, D., Fagerli, H., Jonson, J., Tsyro, S., Wind, P., and Tuovinen, J. P.: Unified EMEP Model Description., Tech. rep., Norwegian Meteorological Institute, 2003. 16055
Solberg, S., Dye, C., Schmidbauer, N., Herzog, A., and Gehrig, R.: Carbonyls and nonmethane hydrocarbons at rural European sites from the Mediterranean to the Arctic, J. Atmos. Chem., 25, 33–66, 1996. 16081, 16082
Talbot, R. W., Bradshaw, J. D., Sandholm, S. T., Smyth, S., Blake, D. R., Blake, N. R., Sachse, G. W., Collins, J. E., Heikes, B. G., Anderson, B. E., Gregory, G. L., Singh, H. B., Lefer, B. L., and Bachmeier, A. S.: Chemical characteristics of continental outflow over the tropical South Atlantic Ocean from Brazil and Africa, J. Geophys. Res., 101, 24187–24202, 1996. 16061
Thompson, A.: The oxidizing capacity of the Earth's atmosphere: Probable past and future changes, Science, 256, 1157–1165, 1992. 16058
Tost, H., Jöckel, P., Kerkweg, A., Sander, R., and Lelieveld, J.: Technical Note: A new comprehensive SCAVenging submodel for global atmospheric chemistry modelling, Atmos. Chem. Phys., 6, 565–574, 2006, http://www.atmos-chem-phys.net/6/565/2006/. 16054
Turquety, S., Logan, J., Jacob, D., Hudman, R., Leung, F., Heald, C., Yantosca, R., Wu, S., Emmons, L., Edwards, D., and Sachse, G.: Inventory of boreal fire emissions for North America in 2004: Importance of peat burning and pyroconvective injection, J. Geophys. Res., 112, D12S03, doi:10.1029/2006JD007281, 2007. 16062
van Aardenne, J., Dentener, F., Olivier, J., Peters, J., and Ganzeveld, L.: The EDGAR 3.2 Fast Track 2000 dataset (32FT2000), http://www.mnp.nl/edgar/model/v32ft2000edgar/docv32ft2000/, 2005. 16054
Van der Werf, G. R., Randerson, J. T., Collatz, G. J., Giglio, L., Kasibhatla, P. S., Avelino, A., Olsen, S. C., and E. S., K.: Continental-scale partitioning of fire emissions during the 1997–2001 El Nino / La Nina period, Science, 303, 73–76, 2004. 16055

Table 1. Distribution of total emissions on 6 emission heights as applied in simulation S1, in Tg(tracegas)/year.

trace gas	emission height in m						total emission	emissions outside the PBL
	45	140	240	400	600	800		
CO	492.11	590.76	3.50	6.17	3.44	0.92	1096.90	207.31
C_2H_4	18.52	7.51	0.09	0.16	0.09	0.02	26.39	2.99
C_2H_6	7.59	4.44	0.13	0.20	0.11	0.02	12.49	1.80
C_3H_6	6.28	3.51	0.04	0.07	0.04	0.01	9.94	1.26
C_3H_8	9.48	1.90	0.18	0.27	0.13	0.03	11.99	1.15
C_4H_{10}	65.09	5.73	1.29	1.92	0.94	0.21	75.17	5.99
MEK	6.05	6.40	0.10	0.17	0.09	0.02	12.82	2.34
CH_3CHO	1.05	2.86	0.01	0.02	0.02	0.00	3.96	0.93
CH_3COCH_3	45.03	2.74	0.07	0.11	0.06	0.01	48.02	2.52
CH_3COOH	6.86	9.16	0.03	0.08	0.06	0.01	16.20	3.10
CH_3OH	68.06	9.39	0.09	0.16	0.10	0.02	77.82	5.39
HCHO	2.67	4.96	0.04	0.07	0.04	0.01	7.79	1.67
HCOOH	7.61	5.00	0.02	0.04	0.03	0.01	12.71	1.83
NO[a]	17.35	14.46	1.35	5.09	3.36	1.53	43.14	10.36

[a] a unit of Tg(N)/year. The total does not include lightning and biogenic sources which are calculated on line (2.1.–2.3 and 6.7–7.0 Tg(N)/year,respectively.

ACPD
9, 16051–16083, 2009

Table 2. Dry deposition of nitrogen compounds in simulation S1 and simulation F1 (in Tg(N)/year).

trace gas	simulation S1		simulation F1	
	wet deposition	dry deposition	wet deposition	dry deposition
NO	–	0.40	–	0.82
NO_2	–	2.93	–	4.69
HNO_3	24.35[a]	13.48	22.53[1]	13.58
PAN	–	0.96	–	0.90
sum (NO_y)	24.35	17.77	22.53	19.99

[a] as nitrate formed from HNO_3.

ACPD
9, 16051–16083, 2009

Table 3. Annual tropospheric ozone budget in Tg for the year 2000. RO2 comprises $C_2H_5O_2$, $CH_3C(O)OO$, $C_3H_7O_2$, $CH_3CH(O_2)CH_2OH$, $CH_3COCH_2O_2$, $C_4H_9O_2$, and peroxy radicals resulting from oxidation of MVK, MEK and isoprene.

	troposphere						planetary boundary layer					
	simulation S1			simulation F1			simulation S1			simulation F1		
	NH	SH	Global	NH	SH	Global	NH	SH	Global	NH	SH	Global
$NO + HO_2$	1887	1248	3135	1854	1242	3096	724	323	1047	704	316	1020
$NO + RO_2$	382	194	576	377	192	569	253	121	374	250	119	369
$NO + CH_3O_2$	683	456	1139	659	446	1105	275	141	416	265	137	402
Total Production	2952	1898	4850	2890	1880	4770	1252	585	1837	1219	572	1791
$O_3 + OH$	−310	−219	−529	−297	−213	−510	−74	−40	−114	−69	−38	−107
$O_3 + HO_2$	−824	−557	−1380	−814	−557	−1371	−208	−110	−318	−203	−108	−311
$H_2O + O^1(D)$	−1422	−1089	−2511	−1404	−1085	−2489	−498	−358	−856	−489	−355	−844
Total Losses	−2556	−1865	−4421	−2515	−1855	−4370	−780	−508	−1288	−761	−501	−1262
net	396	33	429	375	25	400	472	77	549	458	71	529
dry deposition	−507	−273	−780	−488	−268	−756	−507	−273	−780	−488	−268	−756
change in burden	−3	1	−2	2	1	3	1	0	1	1	−1	0
burden	172	150	322	174	151	325	16	9	25	16	8	24
Transport[a]	108	241	349	115	244	359	36	196	232	31	196	227

[a] net downward; derived from budget closure; accounts also for upward transport.

ACPD
9, 16051–16083, 2009

Table 4. Summary of the correlation coefficients (R^2) and linear regression analysis of model results versus aircraft observations (model=m×measurement+b). Bias and b are in pmol/mol; bias=model results minus observations.

		simulation S1				simulation F1				bias ratio	R^2 ratio
trace gas	num. obs.	bias	m	b	R^2	bias	m	b	R^2	(F1/S1)	(F1/S1)
C_2H_4	454	−23.87	0.26	9.97	0.41	−20.39	0.47	4.45	0.51	0.85	1.24
C_2H_6	473	−174.03	0.69	78.69	0.80	−156.7	0.71	82.12	0.80	0.90	1.00
C_3H_6	332	−11.50	0.14	0.27	0.41	−10.36	0.37	−1.84	0.63	0.90	1.54
C_3H_8	472	−18.82	0.92	−5.75	0.77	−13.32	0.94	−4.54	0.76	0.70	0.99
CH_3COCH_3	246	−376.85	0.42	−28.72	0.38	−376.07	0.43	−32.68	0.38	1.00	1.00
CH_3OH	116	−447.82	0.18	255.18	0.31	−452.41	0.20	248.00	0.30	1.01	0.96
HCHO	213	6.41	0.74	55.79	0.63	7.66	0.80	45.16	0.60	1.19	0.95
H_2O_2	411	3.73	0.63	275.81	0.55	26.83	0.65	289.34	0.55	7.19	1.00
HNO_3	416	−13.05	0.53	63.11	0.34	−16.61	0.53	58.34	0.34	1.27	1.00
O_3	506	11835	1.78	-28464	0.54	11740	1.8	-29496	0.53	0.99	0.98
CO	456	−8621.8	0.51	36381	0.63	−7170.6	0.53	35868	0.59	0.83	0.93
NO	417	2.3	0.59	7.75	0.29	−0.61	0.80	4.47	0.30	1.94	1.03

ACPD
9, 16051–16083, 2009

Table 5. Summary of the correlation coefficients and linear regression analysis of model results versus station observations (model=m(×)measurement+b). Bias and b are in nmol/mol; bias=model results minus observations.

		simulation S1				simulation F1				bias ratio	R^2 ratio
trace gas	num. obs.	bias	m	b	R^2	bias	m	b	R^2	(F1/S1)	(F1/S1)
C_2H_4	138	0.20	0.53	0.50	0.40	0.28	0.50	0.60	0.30	1.40	0.75
C_2H_6	150	0.24	0.83	0.54	0.54	0.32	0.77	0.72	0.42	1.33	0.77
C_3H_6	137	0.01	0.66	0.06	0.50	0.03	0.64	0.82	0.41	3.00	0.82
C_3H_8	150	0.61	1.13	0.51	0.42	0.66	1.06	0.62	0.35	1.08	0.83
CH_3CHO	77	0.15	0.20	0.58	0.08	0.14	0.15	0.60	0.04	0.94	0.50
CH_3COCH_3	81	−0.08	0.53	0.46	0.51	−0.09	0.54	0.43	0.47	1.13	0.92
HCHO	65	−0.11	0.47	0.50	0.55	−0.08	0.44	0.55	0.45	0.72	0.81
CO[a]	4224	5.67	0.98	6.50	0.67	9.16	1.00	13.72	0.60	1.61	0.89

[a] from NOAA/ESSL flask sampling network (see Sect. 3.3).

ACPD
9, 16051–16083, 2009

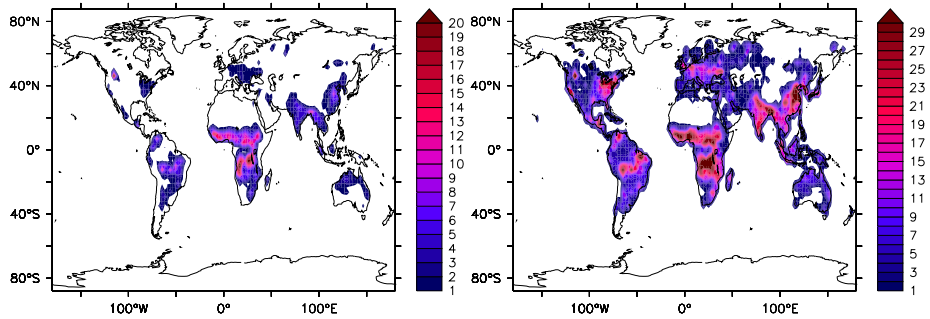

Fig. 1. Left: Annual emissions of CO (in g/m^2) outside the PBL. Right: Total annual emissions of CO (in g/m^2).

ACPD

9, 16051–16083, 2009

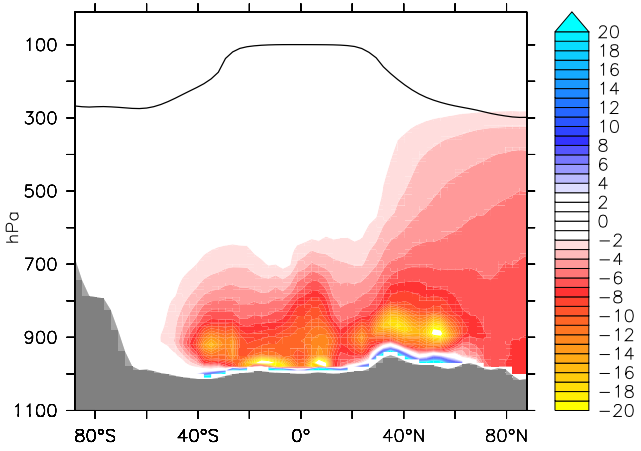

Fig. 2. Annually and zonally averaged relative differences (in %) of NO_y mixing ratios between simulation F1 and simulation S1 ((F1-S1)/S1).

ACPD
9, 16051–16083, 2009

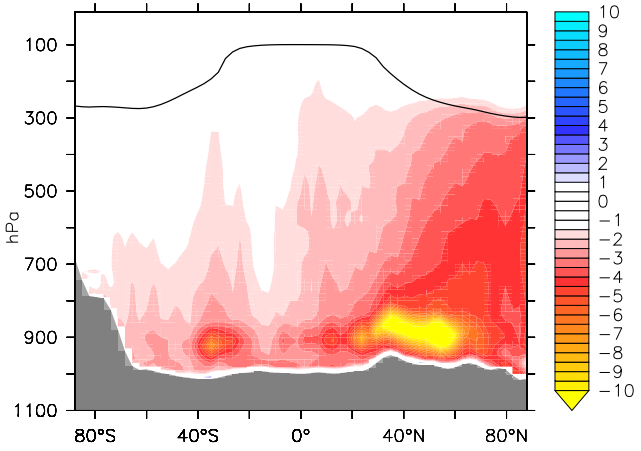

Fig. 3. Annually and zonally averaged relative differences (in %) of OH mixing ratios between simulation F1 and simulation S1 ((F1-S1)/S1).

ACPD

9, 16051–16083, 2009

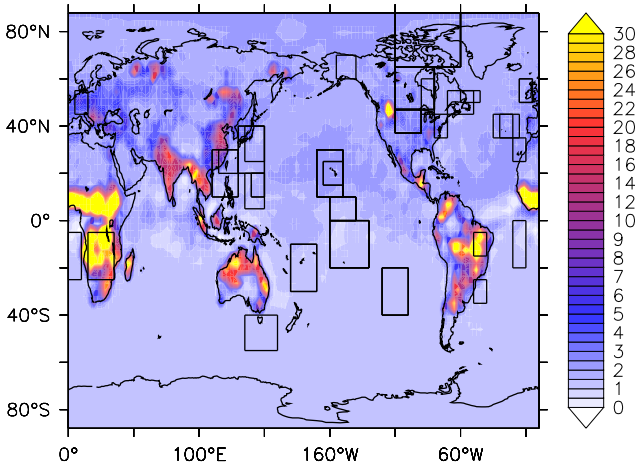

Fig. 4. Annually averaged relative differences (in %) of CO mixing ratios between simulation F1 and simulation S1 ((F1-S1)/S1) at the surface. The overimposed boxes show the regions where the field campaigns used in this study took place.

ACPD
9, 16051–16083, 2009

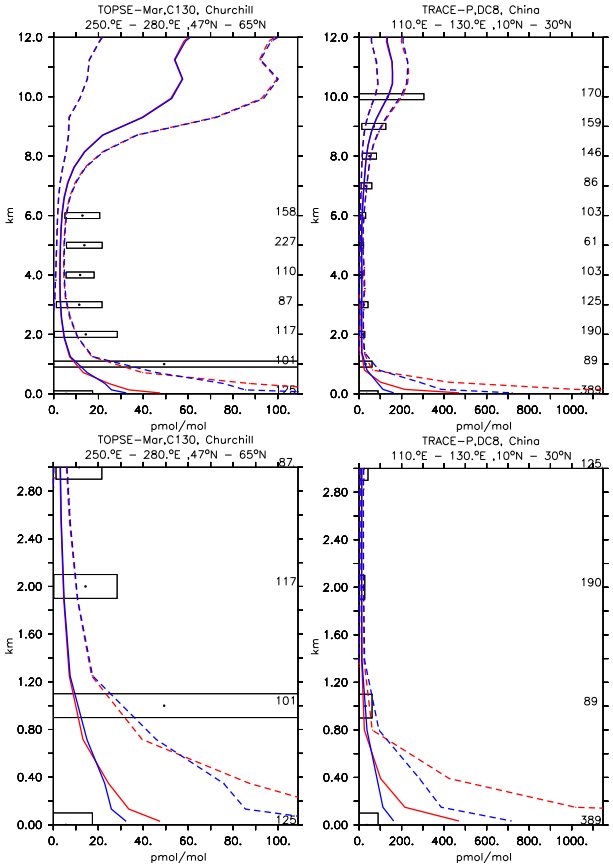

Fig. 5. Vertical profiles of NO (in pmol/mol) for some selected campaigns from Emmons et al. (2000). Asterisks and boxes represent the average and the standard deviation (w. r. t. space and time) of the measurements in the region, respectively. The simulated averages are indicated by the red and blue lines, for simulation F1 and simulation S1 respectively. The corresponding simulated standard deviations w. r. t. time and space are represented by the dashed lines. On the right axis the numbers of measurements are listed. The top and the bottom graphs represent the same data with different vertical axes.

ACPD
9, 16051–16083, 2009

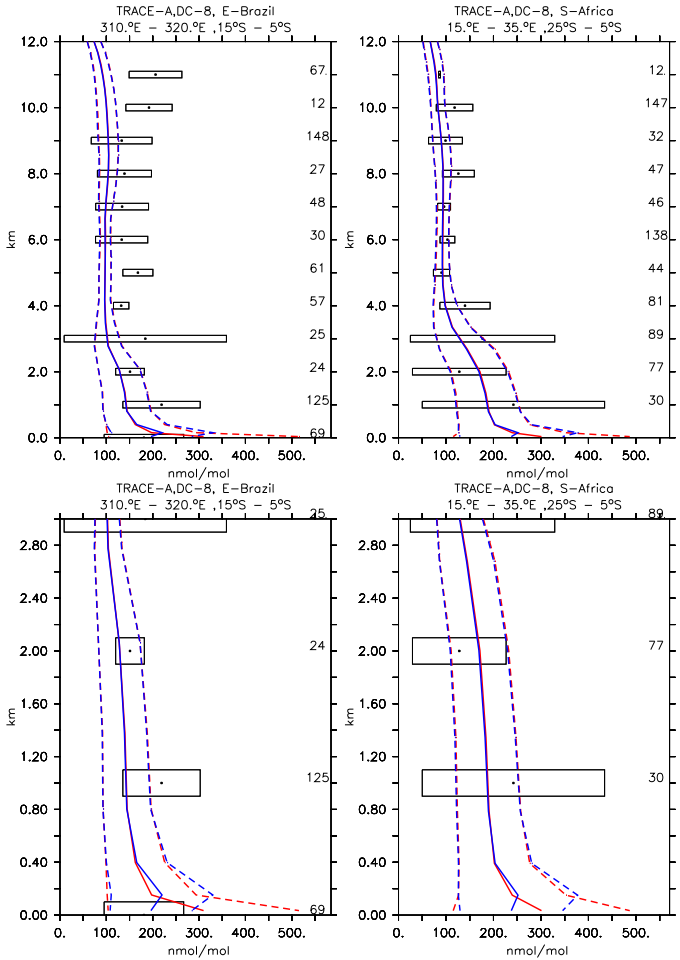

Fig. 6. As Fig. 5 for CO in nmol/mol, for different regions.

ACPD
9, 16051–16083, 2009

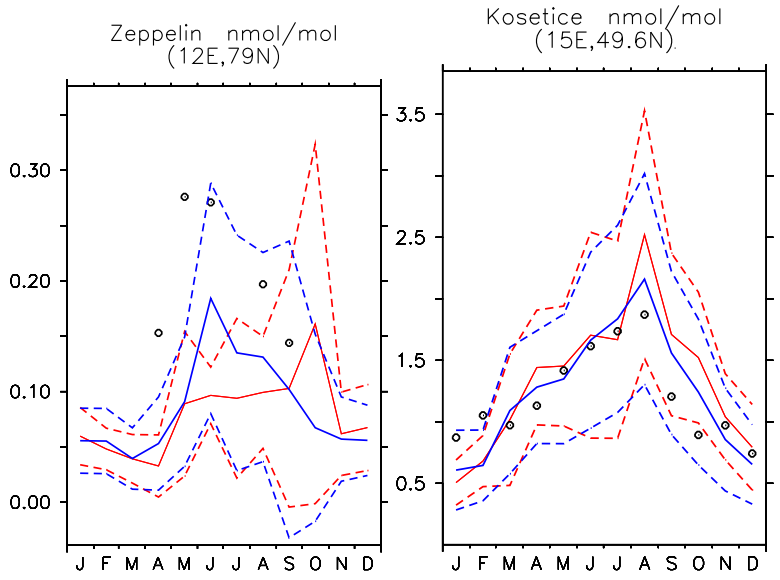

Fig. 7. Seasonal cycle (monthly averages) of HCHO (in nmol/mol) for some selected locations at the surface (Solberg et al., 1996). Model: solid line; model standard deviation: dashed line; measurements: circles. The red and blue lines indicate results from simulation F1 and simulation S1, respectively.

ACPD
9, 16051–16083, 2009

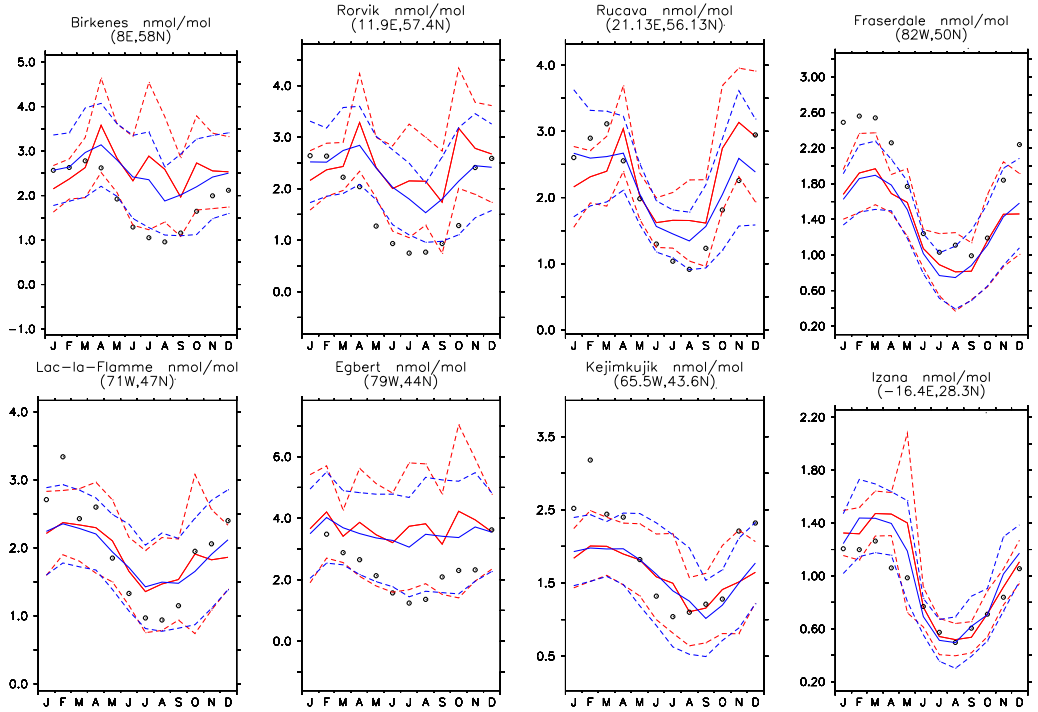

Fig. 8. Seasonal cycle (monthly averages) of C_2H_6 (in nmol/mol) for some selected locations at the surface (Solberg et al., 1996). Model: solid line; model standard deviation: dashed line; measurements: circles. The red and blue lines indicate results from simulation F1 and simulation S1, respectively. The stations are ordered by latitude.

ACPD
9, 16051–16083, 2009

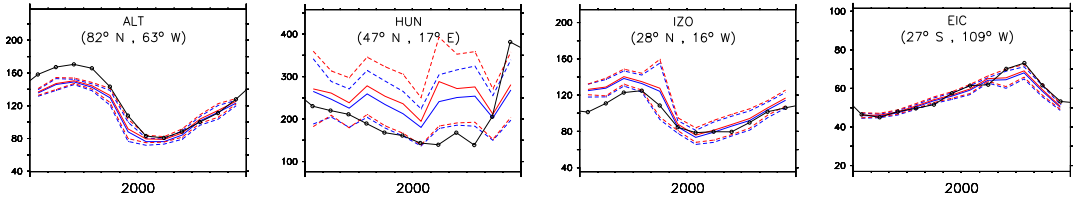

Fig. 9. Comparison of simulated and observed (black, Novelli et al., 1998) CO mixing ratios in nmol/mol (ordered by latitude). The simulated average is indicated by the red and blue lines, for simulation F1 and simulation S1 respectively. The corresponding simulated standard deviations w. r. t. time are represented by the dashed lines.

ACPD
9, 16051–16083, 2009